Supporting Information

Influence of Sorbitol on Protein Crowding in Solution and Freeze-concentrated Phases

S. Khodadadi[1*], N. J. Clark[2,3], A. McAuley[3], V. Cristiglio[4], J. E. Curtis[2],E. Y. Shalaev[5] and S. Krueger[2*]

[1]Faculty of Applied Sciences, Delft University of Technology, Delft, The Netherlands; [2]Center for Neutron Research, National Institute of Standards and Technology, Gaithersburg, MD, USA; [3]Amgen Inc, Thousand Oaks, CA, USA; [4]Institut Laue-Langevin, Grenoble, France; [5]Allergan, Inc., Irvine, CA, USA

Corresponding Authors
*E-mail: s.khodadadi@tudelft.nl; susan.krueger@nist.gov

Materials

Lysozyme from chicken egg white (≥ 90 %) and sorbitol (≥ 98 %) were purchased from Sigma–Aldrich and used without further purification. (Certain commercial equipment, instruments, materials, suppliers, or software are identified in this paper to foster understanding. Such identification does not imply recommendation or endorsement by the National Institute of Standards and Technology, nor does it imply that the materials or equipment identified are necessarily the best available for the purpose.) Exchangeable hydrogen atoms of the sorbitol were exchanged with deuterium by dissolving sorbitol in 99.9% D_2O (Cambridge Isotope Laboratories, Inc.) and freeze-drying the solution to prepare partially deuterated sorbitol. Two samples with different water content but the same weight ratio of sorbitol to lysozyme were prepared. The high water content (HWC) sample contained a D_2O mass fraction of 80 %, a sorbitol mass fraction of 15 % and a lysozyme mass fraction of 5%, while the low water content (LWC) sample contained a D_2O mass fraction of 30 %, a sorbitol mass fraction of 52.5 % and a lysozyme mass fraction of 17.5%. The samples were prepared by first dissolving the desired amount of partially deuterated sorbitol in D_2O.Lysozyme powder was then added in the desired ratio to form the final solution.

Methods

### Small-Angle Neutron Scattering (SANS)

Small-angle neutron scattering (SANS) measurements were performed on the 30 m SANS instruments at the National Institute of Standards and Technology (NIST), Center for Neutron Research (NCNR) in Gaithersburg, MD. The neutron wavelength, λ, was 6 Å, with a wavelength spread of $\Delta\lambda/\lambda \approx 0.15$. The scattered neutrons were detected with a 64 cm × 64 cm two-dimensional position-sensitive detector with 128 × 128 pixels at a resolution of 0.5 cm/pixel. The data were reduced and analyzed using the IGOR program with SANS macro routines developed at the NCNR[1]. The raw counts were normalized to a common neutron intensity and corrected for the empty cell counts, the ambient room background, and the nonuniform detector response. The data obtained from the samples were placed on an absolute scale by normalizing the scattered intensity to the incident beam flux. Finally, the data were radially or sector averaged

to produce the scattering intensity, $I(q)$, vs q curves, where $q = 4\pi\sin\theta/\lambda$ and 2θ corresponds to the scattering angle. Sample-to-detector distances of 12.5 m, 4.0 m, and 1.3 m were used for the measurements to cover the q range between 0.007 Å^{-1} and 0.3 Å^{-1}. The samples were loaded into demountable 1 mm path length titanium cells with titanium windows. The samples were cooled from 298 K to 213 K, 170 K and 100 K and then heated up to 170 K, 213 K and 298 K. The cooling rate was approximately 4 K per minute and the heating rate was approximately 2.6 K per minute. The samples were allowed to remain at each temperature for 30 min before each measurement. Data were recorded for the samples at 1.3 m, 4.0 m, and 12.5 m for 5 min, 10 min, and 15 min, respectively.

For a monodisperse solution of particles, the scattered intensity can be defined as,

$$I(q) = n_p P(q) S'(q), \qquad\qquad (S1)$$

Where n_p is the number density of scattering particles, $P(q)$ is the scattering form factor, which depends on the shape of the particles, and $S'(q)$ is the structure factor, which describes the interactions between particles. For a dilute solution, $S'(q) = 1$ for all q values.
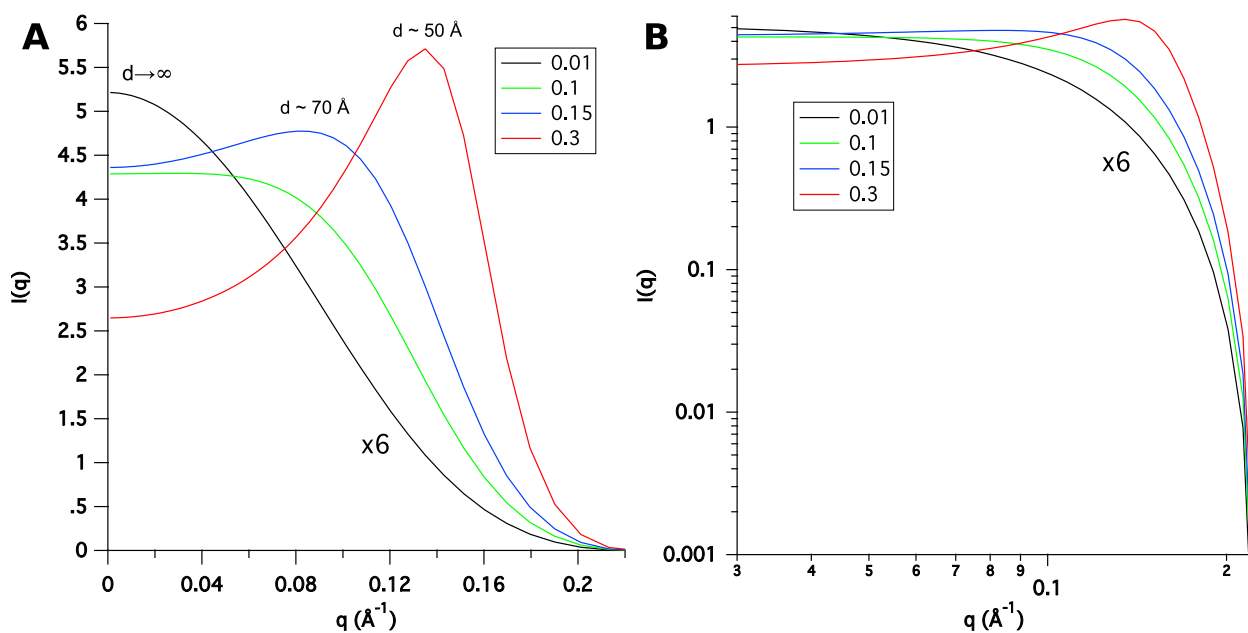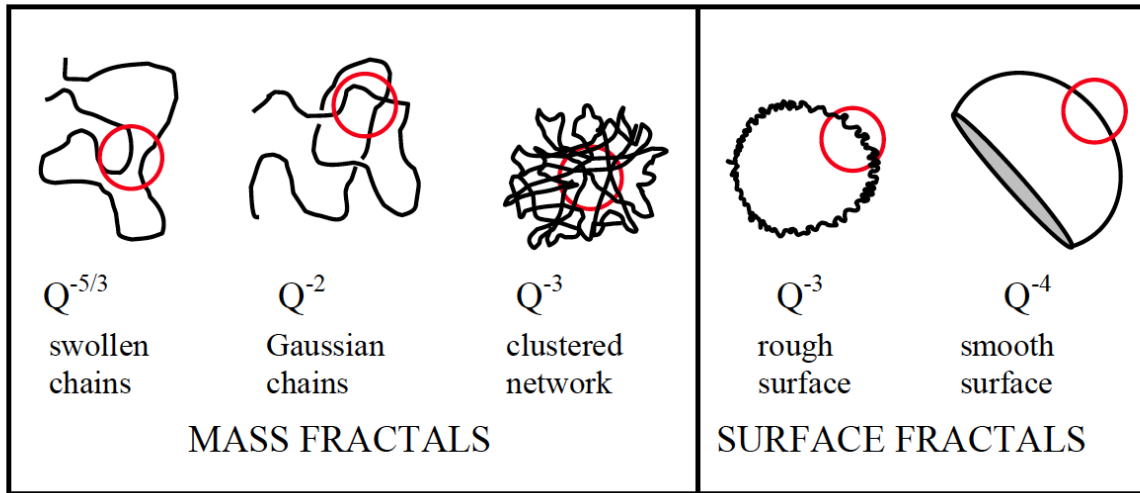

Figure S1. Model SANS $I(q)$ vs q curves for a solution of 40 Å diameter spheres at several different volume fractions, as shown in the legend, interacting via a hard sphere potential, plotted on a A) linear scale and B) log scale. The curve for the volume fraction of 0.01 is scaled by a factor of 6 so that its shape can be seen clearly. The average d-spacing between the centers of mass of the particles is listed above the representative peaks in A).

Figure S1 illustrates the changes in the appearance of $I(q)$ vs q as a solution becomes more concentrated. In this case, $P(q)$ is defined by a 40 Å diameter sphere and $S'(q)$ is defined by the Percus-Yevick[2] hard sphere potential. Calculations were performed using IGOR with NCNR data analysis macro routines[1]. As the volume fraction of spheres increases from 0.01 to 0.3, a

peak appears in the scattering curve and it moves to higher q values with increasing volume fraction. The intensity at lower q values also becomes depressed with respect to the peak height as the volume fraction of spheres increases. The average center of mass distance between the spheres, d, can be approximated by the equation $d = 2\pi/q_0$, where q_0 is the peak position. Thus, the distance between spheres becomes smaller as q_0 becomes larger.

Some systems contain large-scale structures, such as those with interfaces, micelle solutions, suspensions, and other dispersed systems[3]. In such cases, the low q scattering is described by a power law, $I(q)=A/q^n$, where n is fractal dimension as illustrated in Figure S2.

$Q^{-5/3}$	Q^{-2}	Q^{-3}	Q^{-3}	Q^{-4}
swollen chains	Gaussian chains	clustered network	rough surface	smooth surface
MASS FRACTALS			SURFACE FRACTALS	

Figure S2. Schematic representation of structural elements associated with different power law exponents. Taken from Hammouda[4].

Since the data from the lysozyme-sorbitol-water system has both scattering from large-scale structures and from concentrated particles, the SANS data were analyzed using the "broad peak" function in the NCNR IGOR data analysis package. This function describes the scattering intensity at low q with a power law term and the intensity at high q with a term that resembles a Lorentzian function, except that the exponent, m, is not restricted to a value of 2. The equation used to fit the data can be written as,

$$I(q) = \frac{A}{q^n} + \frac{C}{1 + (|q - q_0|\xi)^m} + B. \qquad (S2)$$

Here, A and C are constants, B is a constant background term, n is the power law exponent, q_0 is the peak position, ξ is the Lorentzian screening length, and m is the Lorentzian exponent. Thus, the morphologies of the large-scale structures can be identified on the basis of the power law exponent and the average center of mass distance, d, between the scattering particles can be found based on the peak position.

Table S1. Power law exponent and peak positions for the HWC and LWC during cooling.

Sample	Temperature (K)	n	q_{01} (Å^{-1})	q_{02} (Å^{-1})
HWC	298	3.26 ± 0.01	0.071 ± 0.001	—
HWC	213	3.22 ± 0.01	$\approx 0.07^*$	—
HWC	170	3.40 ± 0.01	$\approx 0.07^*$	$\approx 0.17^*$
HWC	100	3.81 ± 0.01	$\approx 0.07^*$	$\approx 0.17^*$
LWC	298	2.69 ± 0.01	0.071 ± 0.001	$\approx 0.17^*$
LWC	213	3.37 ± 0.01	0.072 ± 0.001	0.166 ± 0.001
LWC	170	3.54 ± 0.01	0.075 ± 0.001	0.167 ± 0.002
LWC	100	3.79 ± 0.01	0.072 ± 0.001	0.167 ± 0.002

*Peak position was estimated directly from the data since the peak intensity is too low to obtain reliable fits to Eq. S2. To obtain q_{02}, n was fixed at 0 and the data were fit beyond $q = 0.12$ Å^{-1}. Errors quoted represent statistical errors from the fit to Eq. S2.

Sub-Ambient Differential Scanning Calorimetry (DSC)

A Perkin Elmer Pyris 1 DSC (PerkinElmer Instruments Norwalk, CT USA) was used with a liquid nitrogen cooling accessory. The instrument was calibrated in the sub-ambient mode using dodecane (mp263.4 K) as a standard. 40 µl of filtered sample was placed in 50 µl semi-hermetically sealed aluminum DSC pans. An empty sealed DSC pan was used as a reference. Samples were loaded into the DSC pans at room temperature and transferred to the DSC cell, also at room temperature. The cooling scan was conducted by lowering the sample temperature from 298K to 193K at the ramp rate of 4 K per minute. The sample was then equilibrated at 193K for 10 minutes and then heated to 298K at a ramp rate of 2.6 K per minute. The resulting thermogram was recorded and baseline optimized using the Perkin Elmer analysis software version 3.81. Subsequently, crystallization temperatures and glass transition temperatures were determined.

The sub-ambient DSC thermograms are shown in Figure S3. The HWC showed a sharp freezing event at 261.25 K during cooling, while two endothermic events, at $T_g' \approx 233$ K and $T_g'' \approx 213$ K, were observed during heating. The physical nature of these two events, which are observed in aqueous solutions of sugars, sugar alcohols, and polymers, is still controversial and a subject of numerous publications[5–13]. The lower-temperature event (so-called T_g'') has been attributed to a glass transition of the freeze-concentrated solution, whereas the second event (T_g') is proposed to be due to either the onset of ice melting/dissolution in the freeze-concentrated solution, or a glass transition of the freeze-concentrate. The LWC did not show a freezing event during cooling, whereas the heating curve shows a crystallization event at 223 K. The DSC results confirm that ice can form in both the HWC and LWC, although the ice nucleation temperature can be expected to be different in the SANS experiment where the larger samples

size would provide more favorable conditions for ice formation. Thus, a freeze-concentrated solution likely exists below 213 K in both samples.

Additional Figures
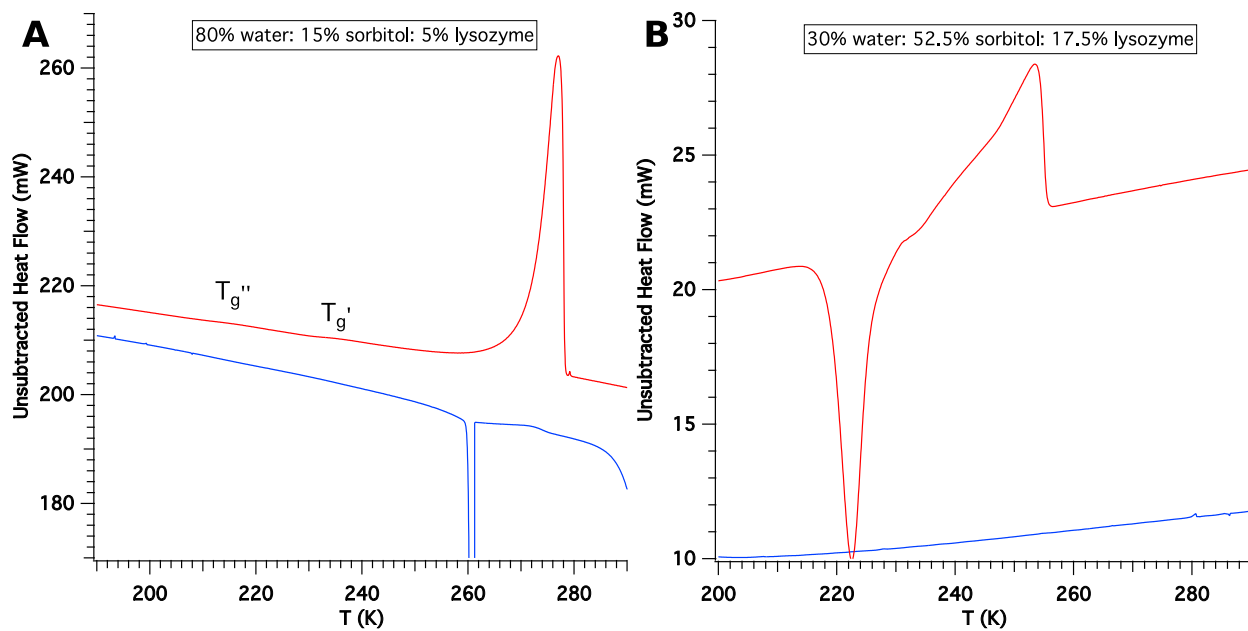
Figure S3. Sub-ambient DSC thermograms for the A) HWC and B) LWC. The cooling curves are shown in blue and the heating curves are shown in red. The glass transition temperatures, $T_g' \approx 233$ K and $T_g'' \approx 213$ K, in A) cannot be easily resolved on this scale. These transitions are obscured by the crystallization event that spans these temperatures in B).
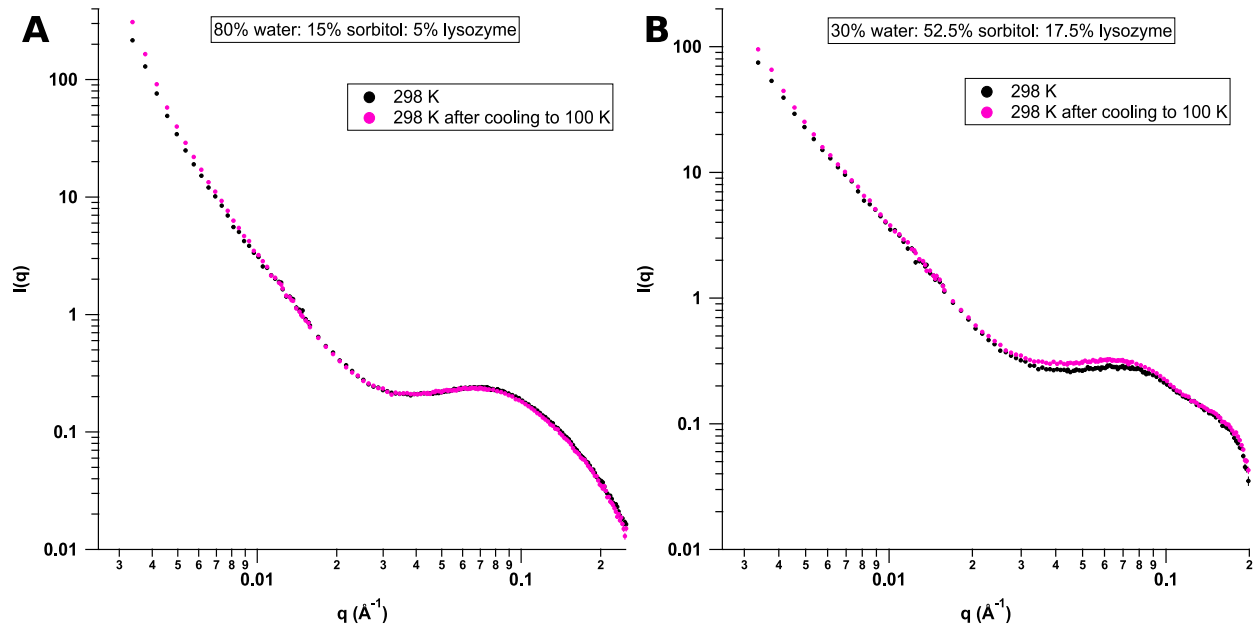
Figure S4. Comparison of SANS scattering profiles at room temperature (298 K) at the beginning and the end of the heating and cooling cycle: A) HWC and B) LWC.

References

1. S. R. Kline, *J. Appl. Crystallogr.*, 2006, **39**, 895–900.
2. J. Percus and G. Yevick, *Phys. Rev.*, 1958, **110**, 1–13.
3. T. Narayanan, in *Soft-matter characterization*, eds. R. Borsali and R. Pecora, Springer, New York, 1st ed., 2008, pp. 899–952.
4. B. Hammouda, .
5. D. Rasmussen and B. Leyet, *Biodynamica*, 1969, **10**, 319–331.
6. A. P. MacKenzie, *Philos. Trans. R. Soc. Lond. B. Biol. Sci.*, 1977, **278**, 167–189.
7. H. Levine and L. Slade, *Carbohydr. Polym.*, 1986, **6**, 213–244.
8. Y. Roos and M. Karel, *J. Food Sci.*, 1991, **56**, 1676–1681.
9. E. Y. Shalaev and F. Franks, *J. Chem. Soc. Faraday Trans.*, 1995, **91**, 1511.
10. H. . Goff, E. Verespej, and D. Jermann, *Thermochim. Acta*, 2003, **399**, 43–55.
11. L. (Lucy) Chang, N. Milton, D. Rigsbee, D. S. Mishra, X. (Charlie) Tang, L. C. Thomas, and M. J. Pikal, *Thermochim. Acta*, 2006, **444**, 141–147.
12. J. Wu, M. Reading, and D. Q. M. Craig, *Pharm. Res.*, 2008, **25**, 1396–1404.
13. H. R. Corti, C. A. Angell, T. Auffret, H. Levine, M. P. Buera, D. S. Reid, Y. H. Roos, and L. Slade, *Pure Appl. Chem.*, 2010, **82**, 1065–1097.